In-Silico Comparison of Phase Maps Based on Action Potential and Extracellular Potential

Konstantin Ushenin[1,2], Artem Razumov[1,2], Vitaly Kalinin[3], Olga Solovyova[1,2]

[1] Ural Federal University, Ekaterinburg, Russia
[2] Institute of Immunology and Physiology, Ekaterinburg, Russia
[3] EP Solution SA, Yverdon-les-Bains, Switzerland

Abstract

In this work, a computer simulation of the reentrant ventricular tachycardia (VT) was used for investigation of peculiar properties of phase maps based on transmembrane potentials (TP) and extracellular potentials (EP). The simulation approach includes the bidomain model with full myocardium-torso coupling, a realistic ionic model of the human cardiomyocytes and personalized geometry of the heart and torso. The phase mapping pipeline includes a signal detrending and the Hilbert transform. It was demonstrated that TP-based phase maps well correlate with the propagation of cardiac excitation. In contrast, EP-based phase mapping provides some aberrations which can complicate electrophysiological interpretation of the phase maps in terms of cardiac activation sequence. It was also shown that a modification of the phase computation algorithm including the sign inversion of signals and a special transformation of the phase plot can partially eliminate those aberrations and make EP-based phase maps more similar to TP-based ones.

1. Introduction

Phase mapping is a widely used approach for signal processing and visualization of reentrant activity in the heart. Initially, the phase mapping was developed for processing of transmembrane potential (TP) signals recorded in ex-vivo optical mapping of the heart [1]. However the TP recording is challenging in humans, and the phase mapping approach was adapted to work with extracellular electrical potential (EP) signals (unipolar electrograms) [2].

This adaptation requires modification of the phase mapping algorithm due to the fact that TP and EP signals have different morphology and electrophysiological nature. In recent works [3, 4], several updates of the phase mapping algorithm are proposed in order to make TP-based phase maps more appropriate for the diagnostic of cardiac arrhythmias. However, the problem of an optimal EP-based phase mapping algorithm is still not solved.

In our study, we use a detailed computer model of reentrant activity in the human ventricles for studying the difference between phase maps based on TP and EP, and propose a modified version the algorithm for EP-based phase mapping which makes EP-based phase maps more similar to TP-based ones.

2. Methods

2.1. Electrophysiology model

The simulation approach is described in our previous work [5]. Briefly, personalized geometry model of the human heart and torso were created using computed tomography data of a patient with the dilated cardiomyopathy. The segmentation and the meshing were performed by Amycard 01 K system (EP solutions SA) and GMSH open source software respectively. Myocardial anisotropy was determined by the rule-based approach. The bidomain model with full myocardium-torso coupling and TNNP model of the human heart ventricular cardiomyocytes [6] were used. Transmural heterogeneity was introduced discretely as the epicardial and endocardial layer with ratio 50:50. Apicobasal heterogeneity was introduced by linear changes of g_{Ks} conductivity from the apex to the base. A reentrant process that served as an in-silico model of polymorphic VT was induced by the virtual pacing using the S1S2 protocol. The tachycardia cycle was 240-260 ms. The core of the single electrical rotor was drifting within a region of 5 cm in diameter in the lateral wall of the left ventricle. The simulation provided TP signals and EP signals (local unipolar electrograms) in each node of the cardiac model. The signals at the time interval from 1650 ms to 3000 ms were selected for the phase processing.

2.2. Phase mapping

The general pipeline for the phase processing of TP and EP signals included band-pass filtering with $(1 - 250$ Hz)

bandpass, signal detrending, and normalization of the signals to the range [-1,1], calculation of instantaneous phase angles and visualization of the results on the myocardium surface. Detrending and normalization of the signals performed by the method, proposed in [7]; the method is based on the determination of the bounds of the signals by upper and lower splines passing through the signal minimal and maximal peaks. Real value TP and EP signals V_k^t and ϕ_k^t were complemented to analytical signals $V_k^t + iH[V_k]^t$ and $\phi_k^t + iH[\phi_k]^t$ respectively by the Hilbert transform . Next, the phase angles were calculated according to the formulas:

$$\mathrm{TP}_k^t = \arctan2(V_k^t, H[V_k^t]), \quad (1)$$

$$\mathrm{EP}_k^t = \arctan2(\phi_k^t, H[\phi_k^t]) \quad (2)$$

where TP_i^t, EP_i^t are phase angle of TP and EP signals respectively. These phase angle definitions are referred to as the basic methods.

In this paper, we also proposed a modified method for calculation of EP signal phases. The method included inversion of the sign of EP signals and the shift of phase plane origin on some vector:

$$\mathrm{EP}_k^t = \arctan2(-\phi_k^t - \alpha, H[-\phi_k^t] - \beta) \quad (3)$$

The algorithm for calculation vector (α, β) is proposed below.

2.3. Calculation of Phase Plane Origin Shift

Fig. 1(a) shows the phase planes with TP and EP analytical signals from 1000 random points of the model. There are several analytical signals that do not encircle the phase plane origin. Proposed algorithm search a point that encircled by a greater number of analytical signal loops that initial phase plane origin.

The main idea is the building of a two-dimensional histogram with the density of all analytical signals on the discretized phase plane. Sequential values of an analytical signal may be placed on a relatively big distance by reason of the signal discretization step. This forces us to present each analytical signal as the polyline and use its points for histogram construction.

Several polylines could pass through the same points on the discretized phase plane. Let us denote the natural logarithm from the number of lines passed through one point as lines per point (LPP) value. Application of the logarithm is suitable here because some points have very high LPP value.

The first part of the algorithm builds an discrete phase plane M with LPP values. Input signals are denoted as S_k^t, $k = 0..N$, $t = 0..T$. The discrete phase plane is

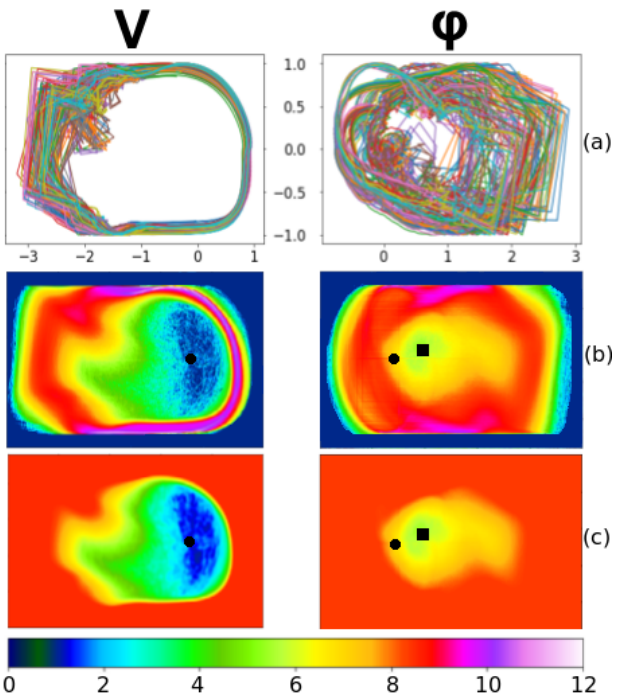

Figure 1. (a) 1000 analytical signals plotted on the same phase plane. (b) All analytical signals plotted on the discrete phase plane M by polylines (logarithmic scale). (c) LPP values for TP and EP phase maps after M postprocessing. A black circle is an initial phase plane origin. A black square is a phase plane origin proposed by the algorithm.

a matrix $i = 1..n, j = 1..m : M_{i,j} = 0$. A function $f : (x+iy) -> ([\rho x + \frac{n}{2} + 1], [\rho y + \frac{m}{2} + 1])$ transforms complex number $x + iy$ into pair of the natural matrix indexes $(a, b) = ([\rho x + \frac{n}{2} + 1], [\rho y + \frac{m}{2} + 1])$, $a, b \in \mathbb{N}$, where $\rho = 10^p$ is a transformation precision, and [] is the rounding operator.

Each analytical signal is presented as a polyline. Bresenham's algorithm transforms each segment of that polyline into the set of points. These sets of points are drawn on the M.

for $k \leftarrow 0..N$ **do**:
  $\{P\}_{j=1}^T \leftarrow \mathrm{Polyline}(f, S_k^t)$
  for P **in** $\{P\}_{j=1}^T$ **do**:
    $\{(a,b)\}_{k=1}^K \leftarrow \mathrm{Bresenham}(P_k)$
    for (a,b) **in** $\{(a,b)\}_{k=1}^K$ **do**:
      $M_{a,b} \leftarrow M_{a,b} + 1$

Results of these processing are shown in Fig.1(b).

The following matrix M processing performed with the goal to make M more suitable for visualization and withdraw from consideration region near to M border. Its includes logarithm transformation of all values (**for** $i = 1..n, j = 1..m : M_{i,j} \leftarrow \ln(M_{i,j})$), and application of

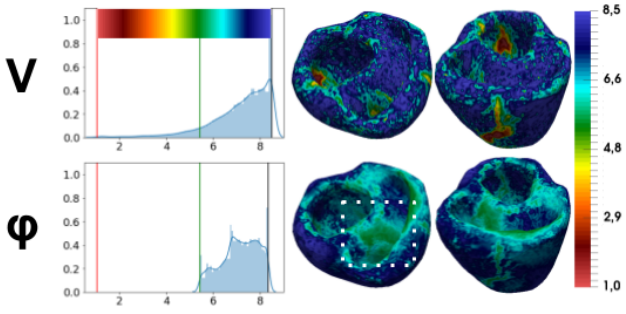

Figure 2. The minimal LPP value distribution and the map of LPP value on the myocardium surface

smoothing and morphological operations to M: gaussian smoothing with σ, and filling border region by h value. Result of this processing is shown in Fig. 1(c). Values of $M_{i,j}$ are lines per point (LPP) values that defined above.

After that threshold cutting with level g performed to M. Thus, we obtain region in the center of M which encircled by the main part of all analytical signals. Center of mass for this region (α, β) is the new phase plane origin proposed by the algorithm.

In the end, each polyline analyzed again with the goal to determine minimal LPP value for each signal source and keeps it in vector $L_k \leftarrow \min_{(a,b)\in\{\{(a,b)\}_{k=1}^{K}\}_{j=1}^{T}} M_{a,b}$.

Point (α, β) and vector L_k are algorithm output values.

3. Results

Phase signals and 3D phase maps calculating by formulas (1) and (2), (3) were compared to each other and to the TM signals and maps. This analysis is focused at a location of the phase fronts on the model surface and position of phase breaks (from $-\pi$ to π or from π to $-\pi$) on the timeline.

The proposed algorithm was applied to TP and EP signals with the following parameters: $\rho = 10^2 = 100$, $h = 8.5$. Matrix with LLP values based on TP had the big free region including the phase plane origin under low threshold level $g = 0.1$. Matrix with LLP values for EP had the small region with center $(\alpha, \beta) = (-0.15, 0.5)$, filled by notable number of analytical signals, under $g = 4$.

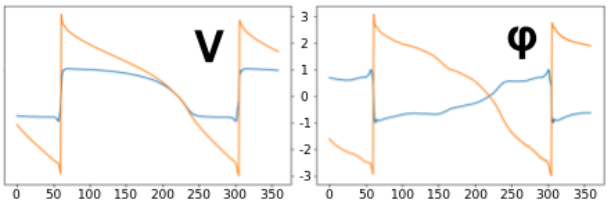

Figure 3. Normalized TP and EP with their phase angle values.

The proposed phase plane origin shift increases the number of loops, encircling the phase plane origin.

Statistical distributions of LPP minimal values for each signal source and its representation on the model surface are shown in Fig. 2. The statistical distributions for TP and EP signals were different, but the similar spatial regularities of LPP minimal values could be traced in both cases: the minimal values of this index were observed in the regions of the rotor core. Also, the region with relatively small minimal LPP values located in septum for EP processing. There are we could expect phase map aberrations.

An example of TP phase angle values as well as an EP phase angle values computed by formulas (1) and (3) are presented in Fig. 3. Maps for each phase angle definition on the myocardium surface are shown in Fig. 4. The phase break of TP phase signals matched with the upstroke of action potentials, i.e. with the moments of the myocardium activation. Mean difference between the phase break and the activation times was 1-3 ms. In contrast to that, phase breaks of EP phase signals computed by the formula (2) did not well matched with a TP upstroke.

Usage of the original phase origin without the (α, β) shift for phase angle computation led to abberation of the phase maps on the model surface. An example of TP based and EP based 3D phase maps are presented in Fig. 4. In contrast to TP based phase maps, EP based phase maps created without the phase plane origin shift have some aberrations that are shown in Fig. 4(e). In particular, there is an observed false phase front (i.e. the front which does not correspond to the front of myocardial depolarization). The application of the shift to phase angle definition (3) made EP-based phase maps more similar to TP-based ones and reduced their aberrations.

4. Discussion and Conclusion

Phase mapping is mainly used for detection and tracking of electrophysiological rotor cores based on the calculation of so-called phase singularities. Nevertheless, the interpretation of phase maps in terms of cardiac activation sequence can be useful for diagnostics of cardiac arrhythmia. Results of this study show that TP based phase maps can provide information about the dynamics of myocardial activation; however, EP based phase maps have aberrations complicating an analysis.

Usage of formulas (1) and (3) provides matching of the TP upstroke with the phase front of the TP based phase map and matching of the EP downstroke with the phase front of the EP based phase map.

Some analytical signal loops may not encircle the origin of the phase plots by reason of significant variability of electrogram shape and amplitude. This issue led to some aberrations on the EP based phase maps complicating its

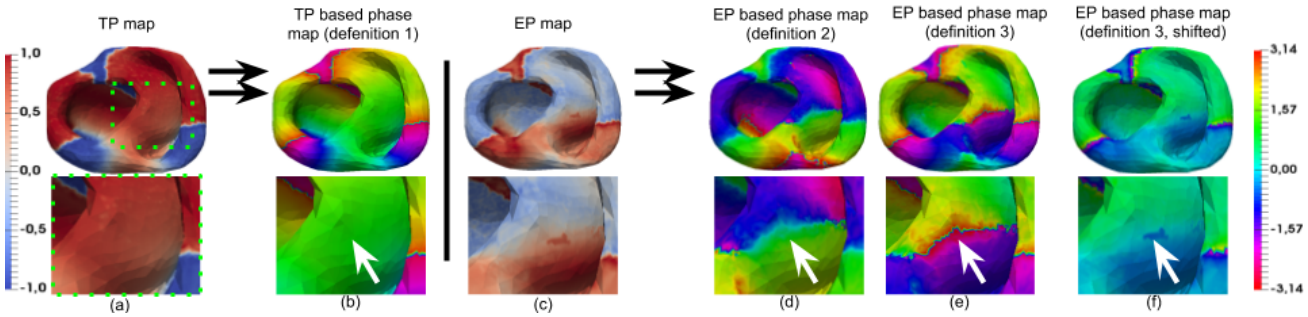

Figure 4. Visualization of results at $t = 2000$ ms. (a) TP map. (b) Phase map based on TP. (c) EP map. (d) Phase map based on EP with abberations. (e) Fixed phase map based on EP.

analysis.

Our preliminary in-silico experiments show that the modification of the phase mapping algorithm including the shift of phase plane origin could reduce the number of those aberrations.

In addition, the LPP index was introduced. We suppose that the index may be useful for analysis of phase mapping algorithms as well as a tool for phase maps interpretation.

Acknowledgements

This work was supported by IIP UrB RAS theme No AAAA-A18-118020590031-8, RF Government Act #211 of March 16, 2013 (agreement 02.A03.21.0006), Program of the Presidium RAS #27 (project AAAA-A18-118020590030-1), RFBR (No. 18-31-00401).

References

[1] Gray RA, Pertsov AM, Jalife J. Spatial and temporal organization during cardiac fibrillation. Nature 1998;392(6671):75.

[2] Clayton RH, Nash MP. Analysis of cardiac fibrillation using phase mapping. Cardiac electrophysiology clinics 2015; 7(1):49–58.

[3] Kuklik P, Zeemering S, Maesen B, Maessen J, Crijns HJ, Verheule S, Ganesan AN, Schotten U. Reconstruction of instantaneous phase of unipolar atrial contact electrogram using a concept of sinusoidal recomposition and hilbert transform. IEEE transactions on biomedical engineering 2015; 62(1):296–302.

[4] Vijayakumar R, Vasireddi SK, Cuculich PS, Faddis MN, Rudy Y. Methodology considerations in phase mapping of human cardiac arrhythmias. Circulation Arrhythmia and Electrophysiology 2016;9(11):e004409.

[5] Ushenin KS, Dokuchaev A, Magomedova SM, Sopov OV, Kalinin VV, Solovyova O, SA ES. Role of myocardial properties and pacing lead location on ecg in personalized paced heart models. Age ;67:56.

[6] Ten Tusscher KH, Panfilov AV. Alternans and spiral breakup in a human ventricular tissue model. American Journal of Physiology Heart and Circulatory Physiology 2006; 291(3):H1088–H1100.

[7] Roney CH, Cantwell CD, Qureshi NA, Chowdhury RA, Dupont E, Lim PB, Vigmond EJ, Tweedy JH, Ng FS, Peters NS. Rotor tracking using phase of electrograms recorded during atrial fibrillation. Annals of biomedical engineering 2017;45(4):910–923.

Address for correspondence:

Ushenin Konstantin Sergeevich
Ural Federal University
620002, 19 Mira street, Ekaterinburg, Russia
konstantin.ushenin@urfu.ru